



Trans. Nonferrous Met. Soc. China 32(2022) 3950-3962

Transactions of Nonferrous Metals Society of China

www.tnmsc.cn



# Microstructure and electrical conductivity of electroless copper plating layer on magnesium alloy micro-arc oxidation coating

Tao LI<sup>1\*</sup>, Zhong-jun LENG<sup>1\*</sup>, Xi-tao WANG<sup>1</sup>, Shi-fang WANG<sup>1</sup>, Su-qing ZHANG<sup>1</sup>, Yuan-sheng YANG<sup>1,2</sup>, Ji-xue ZHOU<sup>1</sup>

- Shandong Provincial Key Laboratory of High Strength Lightweight Metallic Materials, Advanced Materials Institute, Qilu University of Technology (Shandong Academy of Sciences), Jinan 250014, China;
  - 2. Institute of Metal Research, Chinese Academy of Sciences, Shenyang 110016, China

Received 19 September 2021; accepted 14 March 2022

**Abstract:** In order to impart electrical conductivity to the magnesium alloy micro-arc oxidation (MAO) coating, the electroless copper plating was performed. Effects of plating temperature and complexing agent concentration on the properties of the electroless copper plating layers were studied by measuring their microstructure, corrosion resistance and electrical conductivity. It was found that the optimized plating temperature was 60 °C, and the most suitable value of the complexing agent concentration was 30 g/L. Under this condition, a complete and dense plating layer could be obtained. The formation mechanism of the plating layer on magnesium alloy MAO coating was analyzed. A three-stage model of the plating process was proposed. The square resistance of the plated specimen was finally reduced to  $0.03 \Omega$ / after the third stage. Through electroless copper plating, the MAO coated sample obtained excellent electrical conductivity without significantly reducing its corrosion resistance.

Key words: electroless copper plating; electrical conductivity; MAO coating; magnesium alloy

# 1 Introduction

Magnesium alloy has great application potential in engineering and functional fields [1,2]. When it is applied in electronics, petrochemical, and radar communication fields, magnesium alloy devices are required to have not only good corrosion resistance, but also excellent electrostatic discharge capability [3]. Surface coating is considered to be one of the most effective methods to modify the surface characteristics of substrate [4,5]. The micro-arc oxidation (MAO) ceramic coating can greatly improve the corrosion resistance of magnesium alloy [6,7]. However, it

has extremely poor electrical conductivity [8].

In general, there are three methods for surface conductive modification of MAO coating. The first is metal plating, and the common technique is electroless plating [9]. The second is to prepare organic conductive coatings. Specifically, it is divided into intrinsic conductive paint [10] and filled conductive paint [11]. The third is physical deposition coatings. The typical techniques are magnetron sputtering [12] and atomic layer deposition [13]. LI et al [13] fabricated an Al doped ZnO (AZO) film on a MAO coated AZ31 magnesium alloy by using the atomic layer deposition method. The electrical conductivity of the composite coating was increased because of the

<sup>\*</sup>Tao LI and Zhong-jun LENG contributed equally to this work

abundant oxygen deficiency in the AZO film. Among the three types of conductive modified coatings, the conductivity of organic conductive coatings is usually limited, while the physical deposition coatings have poor mechanical properties due to their thinness. The metal plating coating has both excellent electrical conductivity and good mechanical properties.

In fact, there have been many reports on electroless plating on magnesium alloy metal substrates. However, due to the existence of the MAO ceramic intermediate layer on the alloy, the chemical activity of the sample surface is greatly reduced, thus the electroless plating on the magnesium alloy substrate and the MAO coating are completely different. At present, there have been only few studies on MAO treatment followed by electroless plating on magnesium alloy substrates. Even so, the purpose of this two-step treatment was more to take advantage of the dual coating characteristics just to enhance the corrosion resistance of the base alloy [14]. Firstly, the electroless plating layer could seal the micropores in the MAO coating to prevent corrosion by the etching solution. Secondly, the MAO coating could isolate the direct contact between the magnesium substrate and the plating metal, thus eliminating the galvanic corrosion between them [15]. Some only used the MAO coating as an intermediate coating to improve the adhesion of the plating layer [16]. The reason was that the numerous micropores in the MAO coating could provide anchor points for subsequent plating coatings. However, to the best of our knowledge, very few studies focused on the conductive modification of MAO coated magnesium alloy by electroless plating. LI et al [17] prepared an electroless nickel layer on MAO coated AZ31 magnesium alloy. The square resistance was tested, but more in-depth research on the formation mechanism, process optimization and comprehensive performance analysis was not mentioned. On the other hand, expensive palladium was usually used to activate the sample surface before plating in previous studies [18]. In this study, a palladium-free electroless plating technology was used to modify the conductivity of the MAO coating. Previously, since more attention had been paid to the corrosion resistance of composite coatings, nickel-phosphorus coating with better

corrosion resistance was more common than copper or zinc coatings. As for conductivity, copper obviously shows better performance than nickel and zinc. Therefore, copper plating was adopted for conductivity modification in this study.

In the present study, a palladium-free electroless copper plating was performed on the MAO coated magnesium alloy to achieve the conductive character of the specimen. Specific attention was paid to the effects of plating temperature and complexing agent concentration on the microstructure, corrosion resistance, and electrical conductivity of the electroless copper plating layer. Finally, the surface morphology, thickness and electrical conductivity of the copper plating layer during the entire plating process were tracked and tested. And the reaction mechanism and formation mechanism of the electroless copper plating layer on magnesium alloy MAO coating were clarified.

# 2 Experimental

#### 2.1 MAO treatment

Pure Mg (≥99.95%) was chosen for the study because it can be used to obtain a uniform MAO coating to maintain the consistency of the substrate. Pure Mg rolled plates with a thickness of 3 mm were first ground up to 2000 grit and cleaned. A customized bipolar AC pulse power supply device (Jinchuangli AOM7DS, China) was used to conduct MAO treatment. The electrolyte was composed of 3 g/L of NaOH, 10 g/L of Na<sub>2</sub>SiO<sub>3</sub>·9H<sub>2</sub>O and 1.5 g/L of NaF, and the solvent was deionized water. MAO was performed in a constant voltage mode, where the positive phase voltage was 380 V, the negative phase voltage was 90 V, the duty cycle was 10%, the frequency was 500 Hz, and the oxidation time was 5 min.

#### 2.2 Electroless copper plating

Since the MAO coating presented a characteristic of densely arranged micropores, it had an effect of surface roughening. Therefore, the MAO coated specimen was treated as follows. Firstly, the specimen was immersed in the Tollens' reagent of 0.06 mol/L for 2 min for activation treatment. Then, it was immersed in a 40 g/L NaH<sub>2</sub>PO<sub>2</sub> solution for 2 min for reduction treatment. Finally, the specimen was immersed in a preheated plating solution for 30 min for electroless plating.

The plating solution was composed of 8 g/L CuSO<sub>4</sub>·5H<sub>2</sub>O, 15 mL/L HCHO, 12 mL/L CH<sub>3</sub>OH, 50 mg/L K<sub>4</sub>Fe(CN)<sub>6</sub>·3H<sub>2</sub>O and 50 mg/L 2,2'-dipyridine, and 40 g/L NaKC<sub>4</sub>H<sub>4</sub>O<sub>6</sub>·4H<sub>2</sub>O was used as the complexing agent in deionized water. The pH value of the plating solution was adjusted to 12.5. To study the effect of complexing agent concentration, the temperature and plating time were fixed at 60 °C and 20 min, respectively. To obtain the growth curve of the copper layer, specimens were plated at 60 °C with the NaKC<sub>4</sub>H<sub>4</sub>O<sub>6</sub>·4H<sub>2</sub>O concentration of 30 g/L for 0.5–30 min.

#### 2.3 Microstructure characterization

A scanning electron microscope (SEM, Zeiss Evoma10, Germany) equipped with an energy dispersive spectrometer (EDS, Oxford X-Max50, England) was used to examine the surface morphologies. The thicknesses of plating layers were derived from the SEM observations of the longitudinal section of each specimen. An X-ray diffractometer (XRD, Shimadzu 6100, Japan) was adopted to detect the phase constitution of the coating with a scanning rate of 6 (°)/min.

#### 2.4 Corrosion behavior test

The potentiodynamic polarization (PDP) curves were measured in a 3.5 wt.% NaCl solution at room temperature using an electrochemical workstation (Shanghai CH Instrument CHI660E, China). A three-electrode electrochemical cell was used in the measurements, in which a saturated calomel electrode (SCE) was the reference electrode. The PDP curves were measured at a scan rate of 1 mV/s after stabilizing for 2000 s. Immersion tests were conducted by immersing the specimen in a 3.5 wt.% NaCl solution at room temperature. The solution volume to specimen surface area ratio was set to be 10 mL/cm² during the immersion test.

#### 2.5 Electrical conductivity test

The square resistances (*R*) of specimens were measured using a four-point probe meter (Guangzhou Four Probes Tech RTS-9, China). An HP-504 type four-point probe was adopted in the test. The distances between the probes were 1 mm. Each specimen was measured three times and the average value was taken.

# 3 Results and discussion

#### 3.1 Plating temperature

Figure 1 shows the surface morphologies of the original MAO coating and plated specimens performed at different temperatures. As can be seen from Fig. 1(a), the MAO coating presented the typical "crater" accumulation morphology. After plating at 30 °C, only a small number of copper particles were scattered on the surface of the specimen. Most areas of the specimen surface still showed white color of the original MAO base When the plating temperature was coating. increased to 40 °C, much more copper particles were deposited on the surface of the specimen. However, there existed some missing plating areas on the surface of the specimen. The original MAO coating was still faintly visible. On the whole, it still showed obvious incomplete plating. At two lower temperatures of 30 and 40 °C, a complete and dense copper plating layer could not be formed on the MAO coating. While when plating at 50 and 60 °C, things became completely different. After plating, the surfaces of the specimens were completely covered by a dense copper plating layer. Moreover, the specimen surfaces turned to be orange-red with metallic luster. When the plating temperature was further increased to 70 °C, it could be found that the plating solution became very unstable during the plating process. More and more red copper particles were suspended in the plating solution during the plating process. The resulting copper plating layer on the MAO coating therefore became looser.

Figure 2 presents the XRD patterns of plated specimens performed at different temperatures. The results showed that the deposited copper existed in the form of pure copper for all the temperatures. In this study, the overall reaction of the electroless copper plating was presented in Reaction (1) according to Refs. [19,20]. This reaction is an endothermic reaction. At temperatures below 40 °C, the reaction took place more slowly. As a result, it could not generate enough reduced copper to form a dense plating layer. The increase in plating temperature made the reaction easier to take place. At an appropriate temperature of 50–60 °C, copper was reduced at an appropriate rate, and then densely deposited on the surface of the specimen. When the

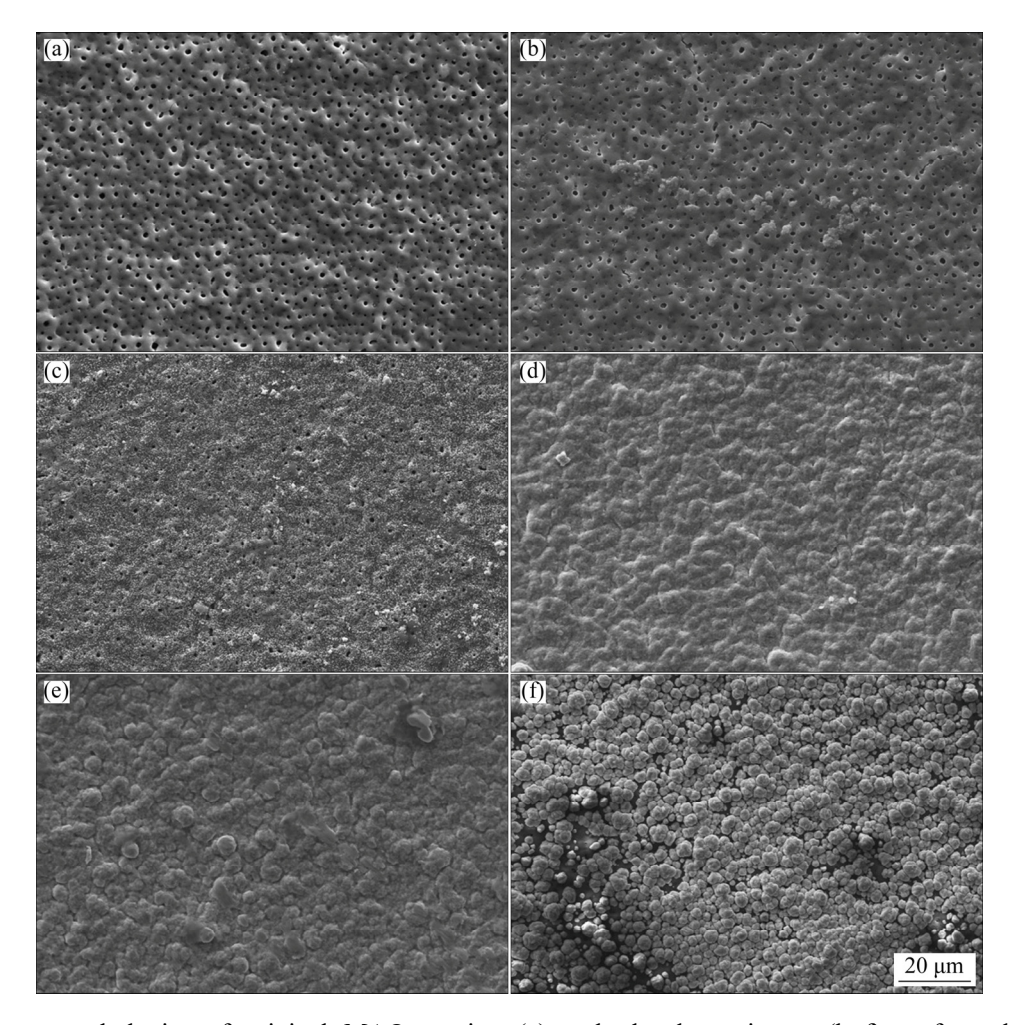


**Fig. 1** Surface morphologies of original MAO coating (a) and plated specimens (b-f) performed at different temperatures: (b) 30 °C; (c) 40 °C; (d) 50 °C; (e) 60 °C; (f) 70 °C

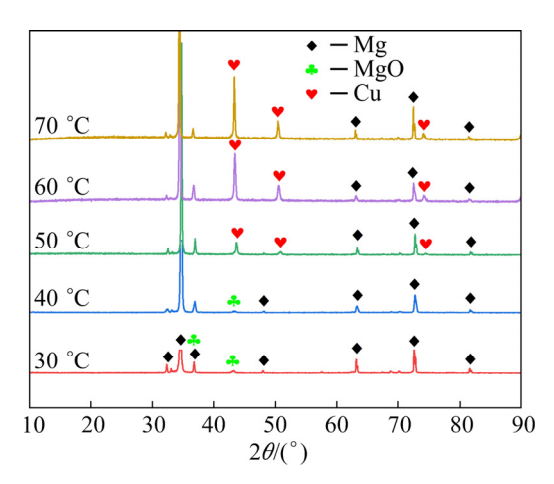


Fig. 2 XRD patterns of plated specimens performed at different temperatures

temperature increased to 70 °C the reaction became too violent. The plating solution suffered serious instability. Copper particles were rapidly reduced in the entire plating solution uncontrollably, and most

of them were suspended in the solution rather than deposited on the surface of the specimen.

$$Cu(C_4H_4O_6)+2HCHO+4OH^-=$$

$$Cu+2HCOO^-+H_2\uparrow+2H_2O+(C_4H_4O_6)^{2^-} \qquad (1)$$

Figure 3 shows the relationship between the square resistance of plated specimens and the plating temperature. For the specimen plated at 30 °C, very few copper particles scattered on the surface of the specimen, and they could not form a continuous conductive channel for electrons, so the specimen maintained the high insulation state of the original MAO ceramic coating. For the specimen plated at 40 °C, although there was a phenomenon of missing plating, the square resistance value of the specimen was greatly reduced due to the formation of the basic conductive channels and the existence of the tunnel effect. As the plating temperature increased, the obtained copper layer

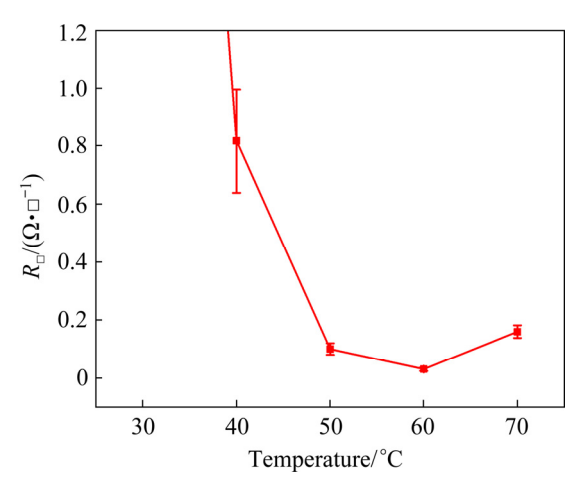


Fig. 3 Relationship between square resistance of plated specimens and plating temperature

became denser and the square resistance value thus became smaller. When the temperature increased to 60 °C, the square resistance value of the specimen reached its minimum. After that, if the temperature continued to rise, the square resistance value of the specimen showed a reverse upward trend due to the decrease in the quality of the copper plating layer.

#### 3.2 Complexing agent concentration

Figure 4 shows the surface morphologies of the plated specimens obtained at different concentrations of the complexing agent. It can be

clearly seen that different concentrations of the complexing agent lead to significant differences in the surface morphologies of the specimens. Both too low (20 g/L) and too high (50 g/L) concentrations of complexing agent resulted in incomplete copper plating and decreased quality of the copper layer. At the concentration of the complexing agent of 30 or 40 g/L, a complete copper plating layer could be formed on the surface of the specimen. In comparison, the copper plating layer formed at 30 g/L of complexing agent was the densest.

When the concentration of the complexing agent was 20 g/L, only about 60% of the surface area of the MAO coating was covered by copper particles. And the surface of each deposited copper particle was rougher compared with those in the other three cases. When the concentration of complexing agent was low, there were some free copper ions without being complexed in the plating solution, and their activity was higher than that of the complexed copper ions. Therefore, the free copper ion underwent reaction as follows:

$$2Cu^{2+}+HCHO+5OH^{-}=Cu_{2}O+HCOO^{-}+3H_{2}O$$
 (2)

Reaction (2) was an incomplete reduction reaction, and the produced Cu<sub>2</sub>O further underwent the following reaction:

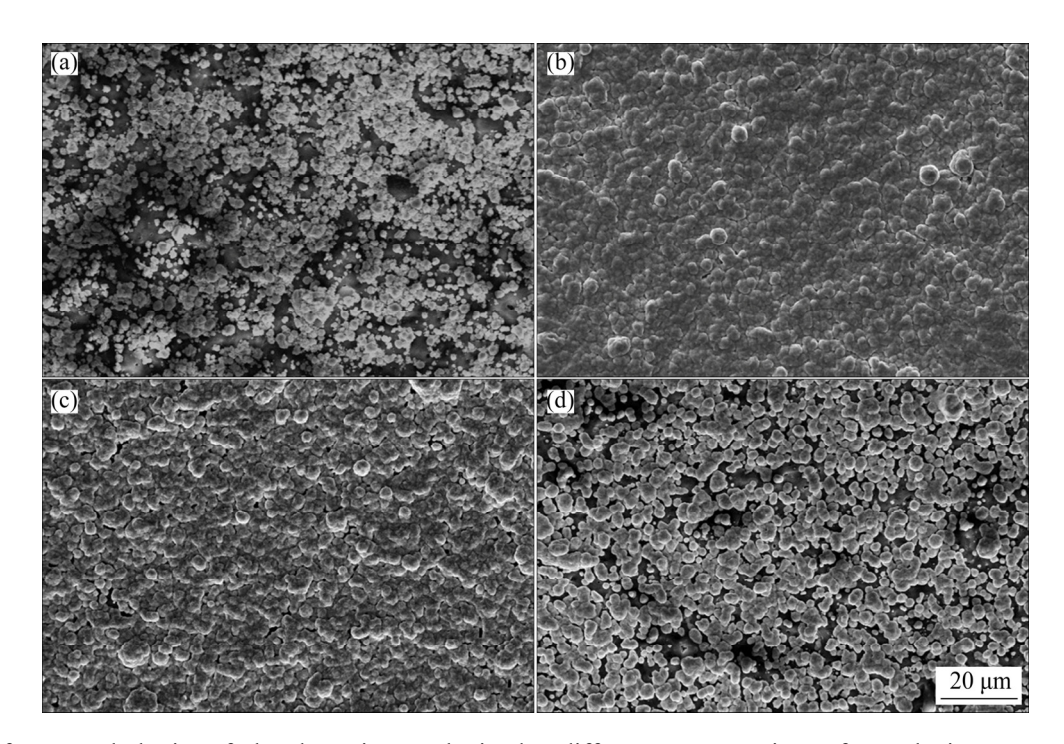


**Fig. 4** Surface morphologies of plated specimens obtained at different concentrations of complexing agent: (a) 20 g/L; (b) 30 g/L; (c) 40 g/L; (d) 50 g/L

 $Cu_2O+2HCHO+2OH^-=2Cu+H_2\uparrow + H_2O+2HCOO^-$ 

(3)

Reactions (2) and (3) occurred in the bath body, so the Cu generated by Reaction (3) was also dispersed in the bath. In fact, Reaction (1) required a catalyst, such as Ag or Cu, to be catalyzed to occur. The ideal plating situation should be that firstly the activated silver catalyzed Reaction (1) to occur on the surface of the specimen, and then the deposited copper continued to catalyze Reaction (1) to occur only on the surface of the specimen. However, due to the occurrence of Reaction (3), a large number of copper particles were also produced in the bath body of the plating solution. These copper particles could also further catalyze Reaction (1) to proceed in the solution body. For these reasons, the reduction rate of copper increased and the stability of the plating solution decreased. This eventually caused a large number of copper particles to be reduced but could not be effectively deposited on the surface of the specimen. The copper particles deposited on the surface of the specimen had a relatively rough surface due to the short inoculation time. Figure 5 presents the XRD patterns of plated specimens obtained at different concentrations of complexing agent. Although Reaction (2) could occur at an inappropriate concentration of the complexing agent, it occurred in the bath body and the intermediate products were finally reduced to copper according to Reaction (3). Therefore, no copper oxide was found in the coating deposited on the specimen surface except for pure copper.

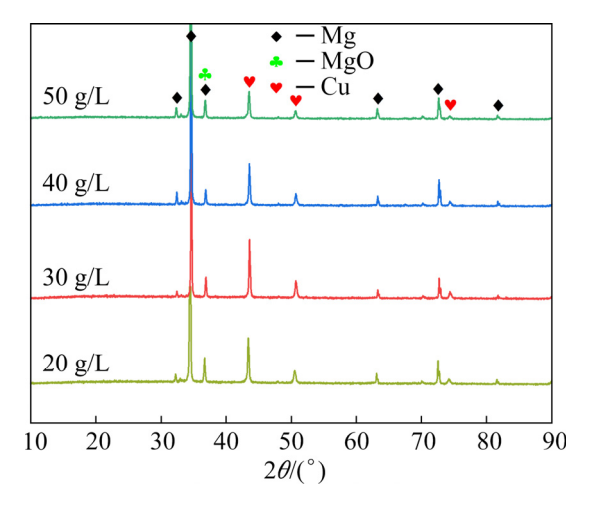


**Fig. 5** XRD patterns of plated specimens obtained at different concentrations of complexing agent

When the concentration of the complexing agent was too high (50 g/L), the complexing agent appeared to be surplus. The excessive organic matter could passivate the deposited copper surface and reduced its catalytic ability. Thus, the overall plating rate decreased. The result was that the plating layer was not dense and the plating was incomplete within a certain period of time.

Figure 6 presents the PDP curves of plated specimens obtained at different concentrations of complexing agent. Table 1 lists the electrochemical data derived from the above PDP curves. As the results show, when the concentrations of the complexing agent were 30 and 40 g/L, self-corrosion potentials  $(\varphi_{corr})$  of the plated specimens were nearly the same, and they were higher than those of the plated specimens which were obtained at the complexing agent concentrations of 20 and 50 g/L. This reflected that the plated specimens related to 30 and 40 g/L of complexing agent showed less susceptible to corrosion [21]. This was attributed to the formation of a complete copper plating layer on the surface of those two specimens. Furthermore, the specimen plated at the complexing agent concentration of 30 g/L exhibited the lowest corrosion current density  $(J_{corr})$ . Besides, it also presented the highest linear polarization resistance  $(R_p)$  compared with the other three specimens. The highest  $R_p$  and the lowest  $J_{corr}$  indicated that under the same environment, Specimen 2 had the lowest corrosion rate. This was mainly because the copper plating layer formed on the surface of the specimen was the densest for the complexing agent concentration of 30 g/L, just as revealed in Fig. 4(b). In addition, it

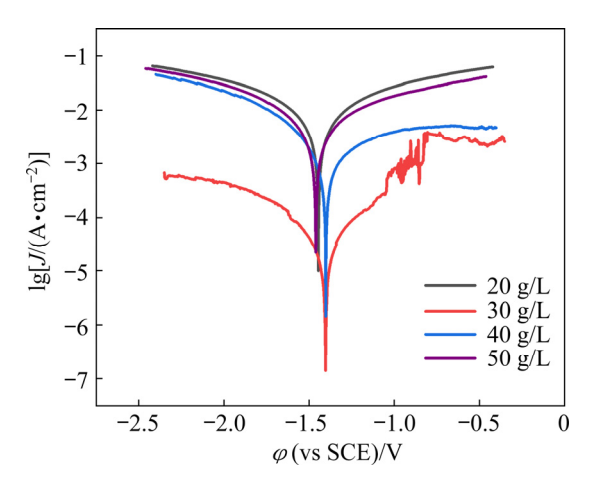


Fig. 6 PDP curves of plated specimens obtained at different concentrations of complexing agent

**Table 1** Electrochemical data of PDP curves

Specimen No.	Complexing agent concentration/ $(g \cdot L^{-1})$	$\varphi_{\rm corr}({ m vs~SCE})/{ m V}$	$J_{ m corr}/({ m A\cdot cm}^{-2})$	$R_{\rm p}/(\Omega\cdot{\rm cm}^2)$
1	20	-1.446	$2.777 \times 10^{-3}$	15.8
2	30	-1.403	$1.564 \times 10^{-5}$	2538.3
3	40	-1.402	$6.555 \times 10^{-4}$	65.6
4	50	-1.461	$1.877 \times 10^{-3}$	23.1

was precisely for this reason that obvious passivation behavior was also found in the anode region of the PDP curve referring to 30 g/L. All these results reflected that the plated specimen, obtained at the complexing agent concentration of 30 g/L, had the strongest corrosion resistance.

Figure 7 shows the relationship between the square resistances of plated specimens and the complexing agent concentrations. For the specimen plated at the complexing agent concentration of 20 g/L, the surface morphology observation showed that most of the surface areas of the MAO coating were covered by copper particles. The basic conductive channels were connected, although the channel might be relatively tortuous. Thus, a moderate value of the square resistance of an order of  $10^1 \Omega$ / was obtained. When the concentrations of the complexing agent were 30 and 40 g/L, the copper plating layer became very dense. And the values of the square resistances were therefore reduced to an order of  $10^{-2} \Omega$ . Considering that the size of the tester probes was much larger than that of the defects in the copper plating layer, a few tiny holes in the plating layer did not visibly affect the square resistance value. Furthermore, both layers basically achieved densification, and the minimal number of defects did not affect the transfixion of

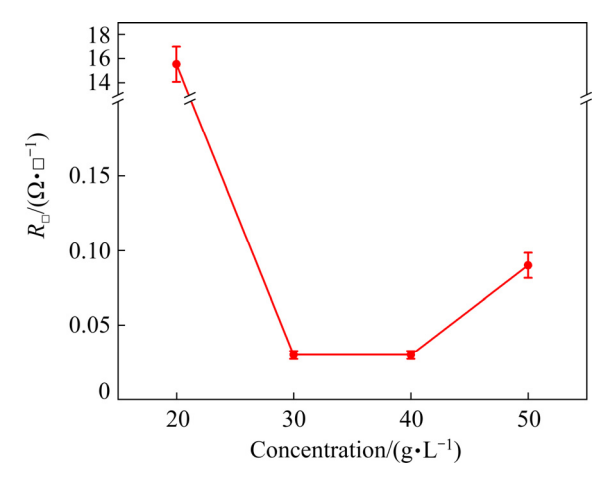


Fig. 7 Relationship between square resistance of plated specimens and complexing agent concentration

the conductive channel. When the concentration of the complexing agent was increased to 50 g/L, the quality of the copper plating layer was significantly deteriorated, as shown in Fig. 4(d). Therefore, the square resistance value was reversed to increase. On the whole, as the concentration of complexing agent increased, the square resistance value first decreased and then increased. When the concentration of the complexing agent was 30 g/L, the plated specimen exhibited both strong corrosion resistance and excellent electrical conductivity.

## 3.3 Microstructure and performance evolution

Figure 8 shows the surface morphologies and EDS results of specimens after plating for different time. After 0.5 min of plating, a small number of scattered copper precipitates could be found on the surface of the sample. As the plating time increased, more and more copper precipitates were deposited on the surface of the sample. Until 2 min, these copper precipitates all appeared to be in a loose state with poor crystal shape. But at the time of 5 min, not only the amount of copper precipitates further increased, but these precipitates aggregated into many compact particles with good crystal shape. Before 5 min, basic occurrence was the precipitation of copper and the inoculation of copper particles. The sample surface was still occupied by a large area of the original MAO coating. At 10 min, the surface of the sample was basically covered by copper particles, and only a small area of the MAO coating was faintly visible. From 5 to 10 min, the copper particles showed significant growth. In the subsequent time, the copper plating layer gradually became complete and was further densified. That is, after 10 min, the main thing that occurred was the densification of the copper plating layer. In summary, the electroless copper plating process on the magnesium alloy MAO coating could be divided into three stages: the first stage occurred in the first 5 min, mainly the inoculation of copper particles; the second stage

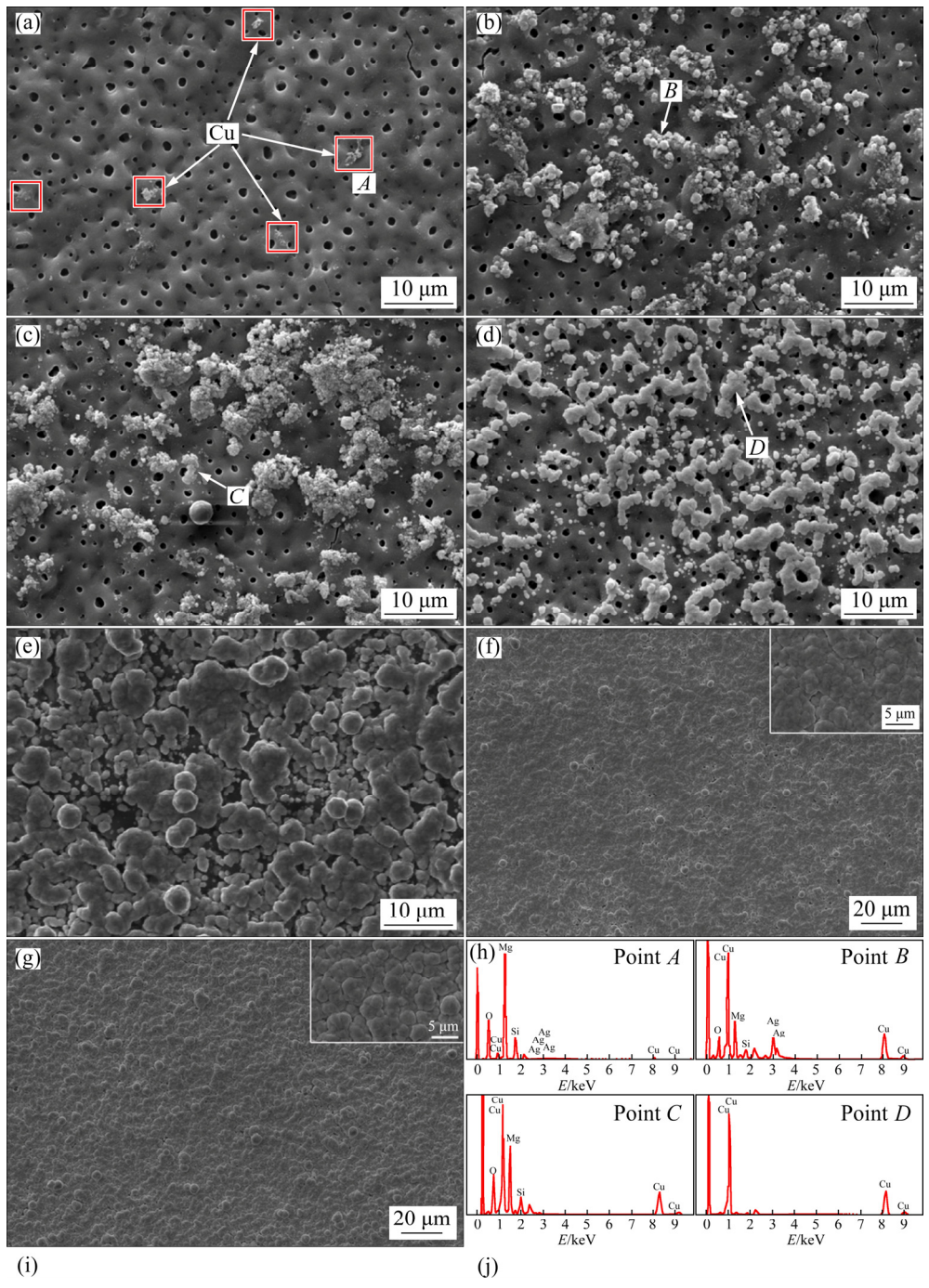


Fig. 8 Surface morphologies (a-g) and EDS results (h) of specimens after plating for different time: (a) 0.5 min; (b) 1 min; (c) 2 min; (d) 5 min; (e) 10 min; (f) 20 min; (g) 30 min

occurred from 5 to 10 min, mainly the growth of copper particles; the third stage occurred after 10 min, mainly the densification of copper plating layer. According to the above discussion, the reaction mechanism and formation mechanism of the electroless copper plating layer on magnesium alloy MAO coating were concluded in the schematic diagram of Fig. 9.

Figure 10 presents the thickness of electroless

copper plating layers as a function of plating time. As analyzed above, in the first 10 min of electroless plating, the inoculation and growth of copper particles mainly occurred. During this period, a complete copper plating layer was not formed. Therefore, the thickness of the copper plating layer was counted as zero until 10 min. Since then, the thickness of the copper plating layer continuously increased. Under the conditions that the effective

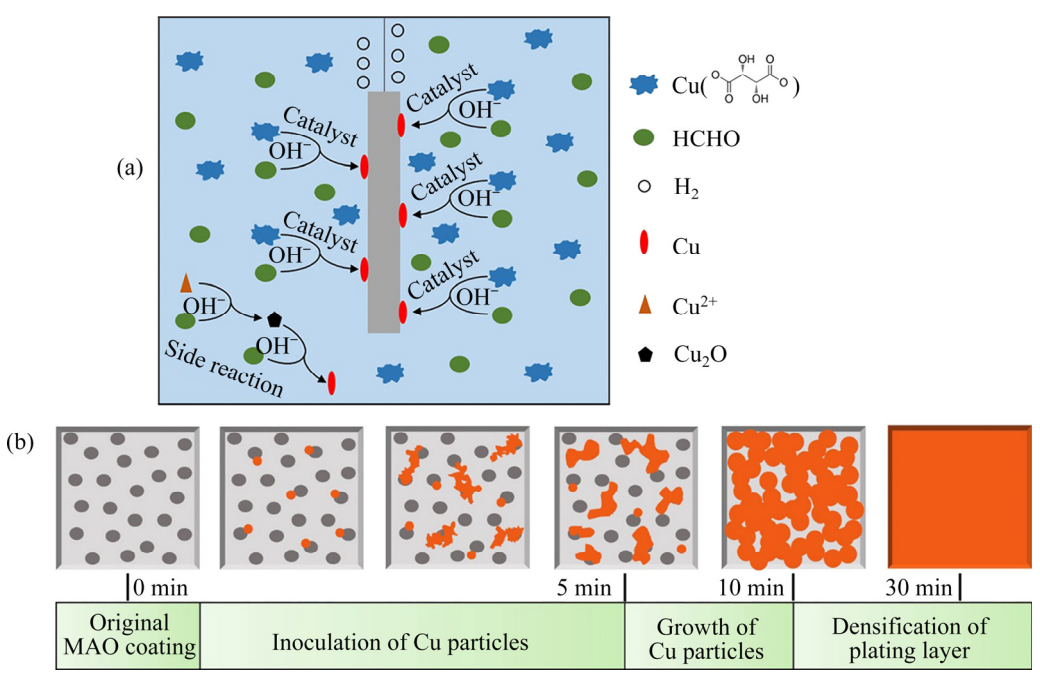
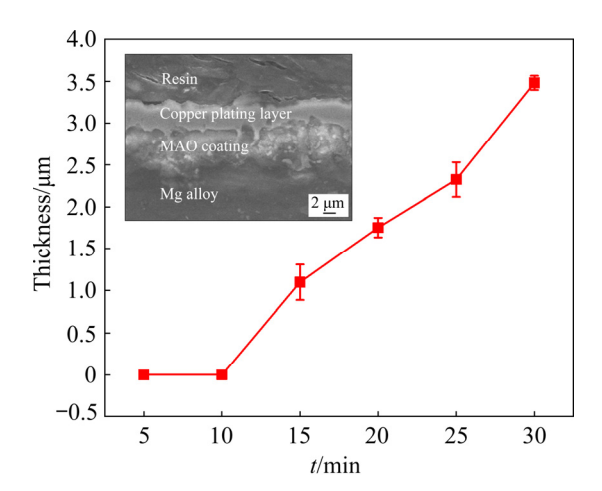


Fig. 9 Schematic diagrams of reaction mechanism (a) and formation mechanism (b) of electroless copper plating layer on magnesium alloy MAO coating



**Fig. 10** Thickness of electroless copper plating layers as function of plating time

components in the plating solution were sufficient, the thickness of the copper plating layer and the plating time were basically linear. Based on this, the target thickness of copper plating layer can be obtained by controlling the plating time. After 10 min, the surface of the sample was almost completely covered by copper. The copper further catalyzed Reaction (1) to continue. Since the number of copper catalytic sites was similarly the same, the reaction rate was nearly constant. And finally, the thickness of the plating layer presented a linear relationship with the plating time. This means that in the third stage of the electroless copper

plating process, the main controlling factor for Reaction (1) was the number of catalytic sites.

Figure 11 shows the square resistances of plated specimens as a function of plating time. Unlike the evolution of thickness, the evolution of square resistance underwent a huge transformation. At the time of 5 min, since a small number of copper particles did not yet form an effective conductive channel, the specimen presented a huge square resistance order of  $10^5 \Omega$ /. As the copper particles grew, when the time came to 10 min, most of the surface areas of the specimen were occupied by copper particles, as shown in Fig. 8(e). As a result, the square resistance of the specimen dropped significantly to the order of  $10^0 \Omega$ . With the densification of the plating layer, the square resistance of the specimen dropped to the order of  $10^{-1} \Omega$ / at 15 min and to the order of  $10^{-2} \Omega$ / at 20 min. Subsequently, although the thickness of the plating layer still increased, the square resistance of the specimen decreased slowly and it finally maintained at  $0.03 \Omega$ /. In summary, the square resistance of the specimen experienced a huge drop in the first two stages, during the first 10 min. This was mainly due to the change of the specimen surface from a highly insulating MAO ceramic coating to a copper plating layer with good electrical conductivity. Since the third stage was

mainly the densification of the copper plating layer, the conductive channels have already been established, so the square resistance was only reduced by two orders of magnitude.

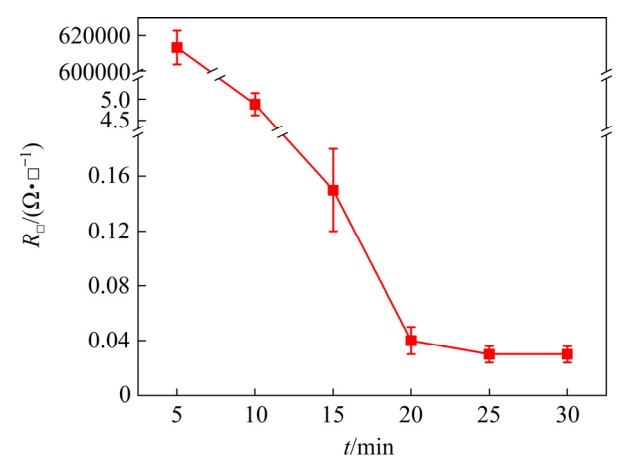


**Fig. 11** Square resistance of plated specimens as function of plating time

#### 3.4 Comprehensive performance

Although the goal of this study was to pursue good electrical conductivity, the corrosion resistance of the material is also crucial in practical applications. Based on this consideration, a comparative study on the corrosion resistance of specimens in different surface states was carried out. Figure 12 shows the PDP curves of bare Mg specimen, MAO coated specimen and MAO/Cu coated specimen. As can be seen, the MAO coated specimen exhibited the highest  $\varphi_{corr}$  and the lowest  $J_{\text{corr}}$ ; while the bare Mg specimen exhibited the lowest  $\varphi_{corr}$  and the highest  $J_{corr}$ . The results of the MAO/Cu coated specimen were somewhere in between. In order to visually demonstrate the corrosion resistance of the three types of specimens, the macroscopic corrosion morphologies after immersion for different time are shown in Fig. 13. After being immersed for 30 min, the bare Mg specimen was severely corroded. At this time, only a small number of corrosion spots appeared at the edges of the MAO/Cu coated specimen, while for the MAO coated specimen, the corrosion sites just emerged. The MAO coated specimen still showed the best corrosion resistance until it was immersed for 500 min. After being immersed for 1000 min, the bare Mg specimen was almost completely corroded, but the difference between the corrosion degree of that of the MAO coated specimen and the MAO/Cu coated specimen was not very significant.

In summary, in a wet environment, electroless copper could induce galvanic corrosion, making the specimen more prone to pitting corrosion. However, for the MAO coated specimen, once the MAO coating was broken down to form corrosion spots, the corrosion would rapidly expand to the surroundings through the magnesium alloy matrix and damage the MAO coating due to volume expansion. Thus, from a long time period, the corrosion resistance of the MAO/Cu coated specimen did not decrease significantly compared with that of the MAO coated specimen.

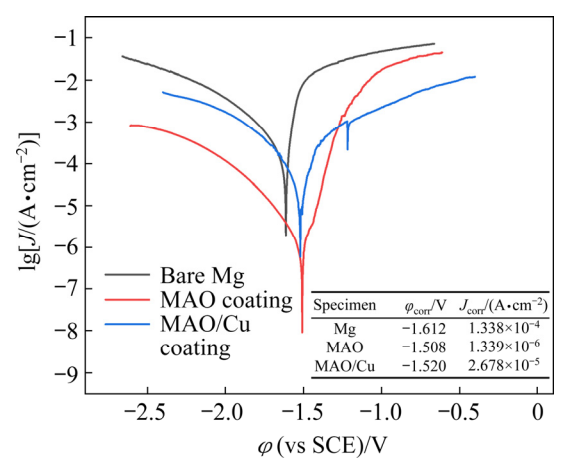


Fig. 12 PDP curves of specimens in different surface states

In this study, after being plated with the copper layer on the magnesium alloy MAO coating, the square resistance of the specimen was finally reduced to  $0.03 \Omega$ /. That shows a perfect electrical conductivity. WANG et al [22] once prepared an electroless copper plating layer on AZ91 magnesium alloy MAO coating, and finally measured the square resistance of the sample to be 0.07  $\Omega$ /. FU and LI [23] prepared electroless nickel plating layers on three different MAO coatings of AZ91 magnesium alloy, and the square resistances of the samples were in the range of  $0.19-2.05 \Omega$ /. Magnetron sputtering can be also used prepare various types of coatings on the substrate. Depending on the type and composition of the coating, it has a wide range of electrical conductivity. VLČEK et al [24] prepared several Zr-B-C-N films with high electrical conductivity on p-type Si(100) or glass substrates by pulsed magnetron sputtering. The square resistances of these films were measured to be  $0.41-0.66 \Omega$ /. While in another work conducted by SHIBATA

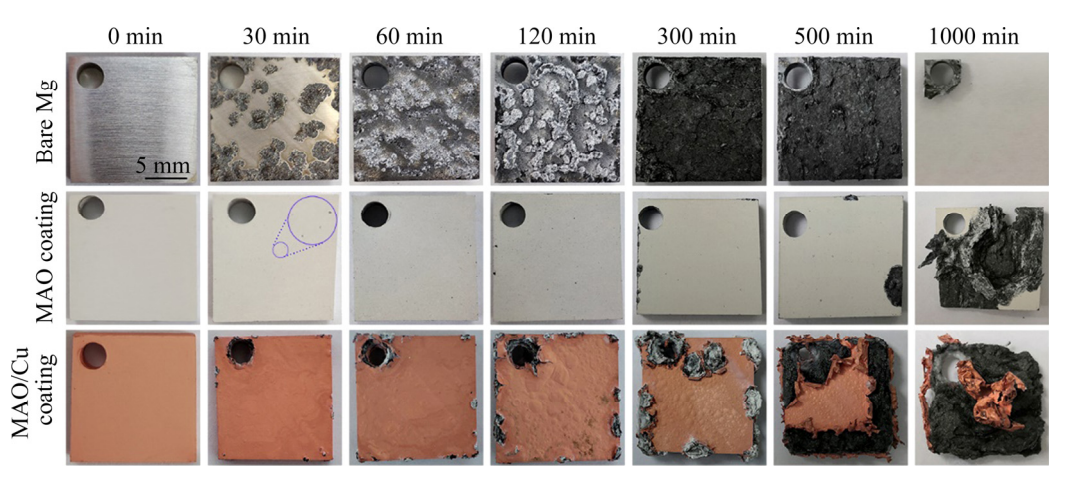


Fig. 13 Macroscopic corrosion morphologies of specimens after immersion for different time

et al [25], silicon-doped diamond-like carbon films were prepared on glass substrates by magnetron sputtering. The square resistance of these films was  $10^4 - 10^6~\Omega/$ . As for conductive polymer coatings, their conductivity is generally poor. Polyaniline is a typical conductive polymer. The square resistances of the polyaniline modified conductive polymer coatings that were also several microns thick could be as high as  $10^6 - 10^{13}~\Omega/$  according to Refs. [26,27]. In summary, in this study, by performing electroless copper plating on the magnesium alloy MAO coating, the sample presented excellent electrical conductivity without significantly reducing its corrosion resistance.

# **4 Conclusions**

- (1) The increasing plating temperature could promote the electroless copper plating reaction, but the stability of the plating solution decreased as the temperature increased. The optimized plating temperature was  $60\,^{\circ}\text{C}$ .
- (2) Too low and too high concentrations of complexing agent caused incomplete plating and decreased quality of the copper layer. At 30 g/L complexing agent, the plated specimen exhibited both strong corrosion resistance and excellent electrical conductivity.
- (3) The electroless copper plating process on the magnesium alloy MAO coating could be divided into three stages with time points of 5 min and 10 min, which were the inoculation of copper particles, the growth of copper particles and the densification of copper plating layer.
  - (4) Through electroless copper plating, the

MAO coated sample obtained an excellent electrical conductivity with a very low square resistance of  $0.03~\Omega/$ . Meanwhile, it exhibited only slightly reduced corrosion resistance.

# **Acknowledgments**

This work was financially supported by the National Key Research and Development Program of China (No. 2016YFB0301105), the National Natural Science Foundation of China (No. 51804190), the Shandong Provincial Natural Science Foundation, China (No. ZR2021ME240), the Youth Science Funds of Shandong Academy of Sciences, China (No. 2020ON0022), the Shandong Province Key Research and Development Plan, China (Nos. 2019GHZ019 and 2019JZZY020329), the Jinan Science & Technology Bureau, China (No. 2019GXRC030), and the Innovation Pilot Project for Fusion of Science, Education and Industry (International Cooperation) from Oilu University of Technology (Shandong Academy of Sciences), China (No. 2020KJC-GH03).

## References

- [1] SONG Y, YANG H B, CHAI Y F, WANG Q H, JIANG B, WU L, ZOU Q, HUANG G S, PAN F S, ATRENS A. Corrosion and discharge behavior of Mg-xLa alloys (x=0.0-0.8) as anode materials [J]. Transactions of Nonferrous Metals Society of China, 2021, 31(7): 1979–1992.
- [2] FU P H, WANG N Q, LIAO H G, XU W Y, PENG L M, CHEN J, HU G Q, DING W J. Microstructure and mechanical properties of high strength Mg-15Gd-1Zn-0.4Zr alloy additive-manufactured by selective laser melting process [J]. Transactions of Nonferrous Metals Society of

- China, 2021, 31(7): 1969-1978.
- [3] GLOR M. Electrostatic ignition hazards in the process industry [J]. Journal of Electrostatics, 2005, 63: 447–453.
- [4] QIU Z M, ZENG R C, ZHANG F, SONG L, LI S Q. Corrosion resistance of Mg-Al LDH/Mg(OH)<sub>2</sub>/silane-Ce hybrid coating on magnesium alloy AZ31 [J]. Transactions of Nonferrous Metals Society of China, 2020, 30(11): 2967-2979.
- [5] NEZAMDOUST S, SEIFZADEH D, HABIBI-YANGJEH A. Nanodiamond incorporated sol-gel coating for corrosion protection of magnesium alloy [J]. Transactions of Nonferrous Metals Society of China, 2020, 30(6): 1535–1549.
- [6] WEI B J, CHENG Y L, LIU Y Y, ZHU Z D, CHENG Y L. Corrosion and wear resistance of AZ31 Mg alloy treated by duplex process of magnetron sputtering and plasma electrolytic oxidation [J]. Transactions of Nonferrous Metals Society of China, 2021, 31(8): 2287–2306.
- [7] DAVOODI F, ATAPOUR M, BLAWERT C, ZHELUD-KEVICH M. Wear and corrosion behavior of clay containing coating on AM 50 magnesium alloy produced by aluminate-based plasma electrolytic oxidation [J]. Transactions of Nonferrous Metals Society of China, 2021, 31(12): 3719–3738.
- [8] LI C Y, FAN X L, CUI L Y, ZENG R C. Corrosion resistance and electrical conductivity of a nano ATO-doped MAO/ methyltrimethoxysilane composite coating on magnesium alloy AZ31 [J]. Corrosion Science, 2020, 168: 108570.
- [9] ZHANG P P, LV Z, LIU X, XIE G, ZHANG B Q. Electroless nickel plating on alumina ceramic activated by metallic nickel as electrocatalyst for oxygen evolution reaction [J]. Catalysis Communications, 2021, 149: 106238.
- [10] GUO X G, FACCHETTI A. The journey of conducting polymers from discovery to application [J]. Nature Materials, 2020, 19(9): 922–928.
- [11] MONDAL R K, DUBEY K A, BHARDWAJ Y K. Role of the interface on electron transport in electro-conductive polymer-matrix composite: A review [J]. Polymer Composites, 2021, 42(6): 2614–2628.
- [12] WANG Z H, BAI L J, WANG A L, ZHANG G J. Microstructure and properties of duplex coating on AZ91 magnesium alloy combined with MAO and magnetic sputtering copper [J]. Rare Metal Materials and Engineering, 2018, 47(8): 2561–2566. (in Chinese)
- [13] LI Y, LI H, XIONG Q Y, WU X M, ZHOU J, WU J Z, WU X, QIN W. Multipurpose surface functionalization on AZ31 magnesium alloys by atomic layer deposition: Tailoring the corrosion resistance and electrical performance [J]. Nanoscale, 2017, 9(25): 8591–8599.
- [14] CHEN Q, ZHENG Y, DONG S, CHEN X B, DONG J. Effects of fluoride ions as electrolyte additives for a PEO/Ni-P composite coating onto Mg alloy AZ31B [J]. Surface and Coatings Technology, 2021, 417: 126883.
- [15] SONG Z W, XIE Z, YU G, HU B, HE X N, ZHANG X Y. A novel palladium-free surface activation process for electroless nickel deposition on micro-arc oxidation film of AZ91D Mg alloy [J]. Journal of Alloys and Compounds,

- 2015, 623: 274-281.
- [16] SHAO Z L, JIANG H T, WEI S Q, WU L P. Structure and performance of electroless nickel plating combined with micro-arc oxidation on pure titanium [J]. Advanced Science Letters, 2011, 4(3): 750–754.
- [17] LI J M, ZHANG Q, CAI H, WANG A, ZHANG J M, HUA X H. Controlled deposition, electrical and electrochemical properties of electroless nickel layers on microarc oxidized magnesium substrates [J]. Materials Letters, 2013, 93: 263–265.
- [18] SHANG W, ZHAN X Q, WEN Y Q, LI Y Q, ZHANG Z, WU F, WANG C L. Deposition mechanism of electroless nickel plating of composite coatings on magnesium alloy [J]. Chemical Engineering Science, 2019, 207: 1299–1308.
- [19] de LUNA M D G, CAPITO J A, VILANDO A C, LU M C. Effect of EDTA and CH<sub>2</sub>O on copper recovery from simulated electroless copper plating spent rinse water by unseeded fluidized-bed granulation process [J]. Separation and Purification Technology, 2020, 253: 117460.
- [20] LIN S H, KAO H C, SU H N, JUANG R S. Effect of formaldehyde on Cu(II) removal from synthetic complexed solutions by solvent extraction [J]. Journal of Hazardous Materials, 2005, 120(1): 1–7.
- [21] LI T, HE Y, WU J H, ZHOU J X, TANG S Q, YANG Y S, WANG X T. Effects of scandium addition on the in vitro degradation behavior of biodegradable Mg-1.5Zn-0.6Zr alloy [J]. Journal of Materials Science, 2018, 53(20): 14075-14086.
- [22] WANG Z H, ZHANG J M, BAI L J, ZHANG G J. Microstructure and property of composite coatings on AZ91 Mg-alloy prepared by micro-arc oxidation and electroless Cu-layer [J]. Journal of Chinese Society for Corrosion and Protection, 2018, 38(4): 391–396. (in Chinese)
- [23] FU M, LI J M. Surface modification of microarc oxidation combined with electroless nickel plating for magnesium alloys [J]. Materials Protection, 2019, 52(6): 79–83. (in Chinese)
- [24] VLČEK J, STEIDL P, KOHOUT J, ČERSTVÝ R, ZEMAN P, PROKŠOVÁ Š, PEŘINA V. Hard nanocrystalline Zr–B–C–N films with high electrical conductivity prepared by pulsed magnetron sputtering [J]. Surface and Coatings Technology, 2013, 215: 186–191.
- [25] SHIBATA Y, KIMURA T, NAKAO S, AZUMA K. Preparation of silicon-doped diamond-like carbon films with electrical conductivity by reactive high-power impulse magnetron sputtering combined with a plasma-based ion implantation system [J]. Diamond and Related Materials, 2020, 101: 107635.
- [26] QI L, XIE A, CHEN T J, HAN J, YU L, ZHANG M. Direct access to xylene solution of polyanilines via emulsion polymerization-extraction method facilitating the preparation of conductive film materials [J]. Materials Letters, 2019, 254: 361–363.
- [27] BHADRA J, AL-THANI N. Advances in blends preparation based on electrically conducting polymer [J]. Emergent Materials, 2019, 2(1): 67–77.

# 镁合金微弧氧化涂层上化学镀铜层的 显微组织和导电性

李涛1,冷中军1,王西涛1,王世芳1,张素卿1,杨院生1,2,周吉学1

1. 齐鲁工业大学(山东省科学院)新材料研究所 山东省轻质高强金属材料省级重点实验室,济南 250014; 2. 中国科学院 金属研究所,沈阳 110016

摘 要:为了赋予镁合金微弧氧化(MAO)涂层以导电特性,对 MAO 涂层进行化学镀铜处理。通过测试镀层的显微组织、耐蚀性和导电性,研究镀覆温度和络合剂浓度对化学镀铜层性能的影响。结果表明,最优镀覆温度为  $60\,^{\circ}\mathrm{C}$ ,最佳络合剂浓度为  $30\,\mathrm{g/L}$ 。在此条件下,可获得完整、致密的镀层。分析镀层在镁合金 MAO 涂层上的形成机制,提出镀覆过程的三阶段模型。镀后试样的表面方阻在经历第三阶段后降低至  $0.03\,\Omega$ / 。通过化学镀铜,MAO 样品在未明显降低耐蚀性的同时获得了良好的导电性。

关键词: 化学镀铜; 导电性; MAO 涂层; 镁合金

(Edited by Wei-ping CHEN)